IBRACON Structures and Materials Journal
Revista IBRACON de Estruturas e Materiais
ISSN 1983-4195 ismj.org

ORIGINAL ARTICLE

Development of alkali-activated mortar from iron ore tailings

Desenvolvimento de argamassas álcali ativadas a partir de rejeito de barragem de minério de ferro

Keoma Defáveri do Carmo e Silva[a]
Fernanda Pereira da Fonseca Elói[b]
José Maria Franco de Carvalho[c]
Ricardo André Fiorotti Peixoto[b]
Guilherme Jorge Brigolini Silva[b]

[a]Universidade Federal de Lavras – UFLA, Laboratório de Pavimentação, Lavras, MG, Brasil
[b]Universidade Federal de Ouro Preto – UFOP, Laboratório de Materiais de Construção Civil, Ouro Preto, MG, Brasil
[c]Universidade Federal de Viçosa – UFV, Laboratório de Materiais Compósitos, Viçosa, MG, Brasil

Received 16 August 2022
Accepted 12 December 2022

Abstract: In this work, the authors explore the use of iron ore tailings (IOT) from a tailings dam as a recycled precursor material in producing a composite through alkali-activation technology. Two different composite types were evaluated: paste specimens made using only IOT and an alkaline activator, and mortar specimens using the same binder and quartz sand as fine aggregate. Three different grinding times were applied to activate the IOT; a NaOH solution was used as the alkaline activator with three molar concentrations (8, 10, and 12 mol/l); and, thermal curing of 100°C for 7 days was applied. These parameters were obtained by a hard-mini-test (HMT) experimental procedure. The physico-mechanical properties of the composites were obtained, and the results showed a compressive strength up to 110.0 MPa, which is like high-performance Portland cement concretes and alkali-activated cements derived from well-established precursors reported in the literature using thermal cure.

Keywords: alkali-activated, iron ore tailings, compressive strength, composite.

Resumo: Neste trabalho, os autores exploram o uso do rejeito de barragem de minério de ferro (RBMF), de uma barragem de rejeitos, como material precursor reciclado na produção de um compósito através da tecnologia de ativação alcalina. Dois compósitos diferentes foram avaliados: espécimes de pastas feitas usando somente RBMF e ativador alcalino, e espécimes de argamassa usando o mesmo aglomerante e areia como agregado miúdo. Três tempos de moagem diferentes foram aplicados para ativar o RBMF; uma solução de NaOH foi empregada como ativador alcalino com três concentrações molares (8, 10 e 12 mol/l); e cura térmica de 100ºC por 7 dias. Esses parâmetros iniciais foram obtidos através do procedimento experimental Endurecimento-Mini-Teste (EMC). As propriedades físico-mecânicas dos compósitos foram determinadas e os resultados mostraram uma resistência a compressão de até 110,0 MPa, que é compatível com concreto de cimento Portland de alto desempenho e cimentos álcali-ativados feitos a partir de precursores bem estabelecidos reportados na literatura usando cura térmica.

Palavras-chave: álcali-ativado, rejeito de barragem de minério de ferro, resistência à compressão, compósito.

How to cite: K. D. C. Silva, F. P. F. Elói, J. M. F. Carvalho, R. A. F. Peixoto, and G. J. B. Silva, "Development of alkali-activated mortar from iron ore tailings," *Rev. IBRACON Estrut. Mater.*, vol. 16, no. 5, e16506, 2023, https://doi.org/10.1590/S1983-41952023000500006

1 INTRODUCTION

Alkali-activated cements can be defined as mineral polymer materials produced by the alkali activation of aluminosilicate materials. These materials belong to the same family of aluminosilicates as zeolites, although they are

Corresponding author: Keoma Defáveri do Carmo e Silva. E-mail: keoma.silva@ufla.br
Financial support: Coordenação de Aperfeiçoamento de Pessoal de Nível Superior (CAPES), Fundação de Amparo a Pesquisa de Minas Gerais (FAPEMIG).
Conflict of interest: Nothing to declare.
Data Availability: The data that support the findings of this study are available from the corresponding author, KD, upon reasonable request.

essentially amorphous polymers or nanocrystals, unlike zeolites. The alkali activation occurs in a highly concentrated alkaline environment – yielded by a strong alkaline solution (e.g., potassium hydroxide or sodium hydroxide) and solid alkali activator (e.g., sodium metasilicate or sodium aluminate) – where the aluminosilicate starting material works as a precursor to the formation of a polymeric structure formed by interconnected Si-O-Al bonds. The starting materials dissolve in a high pH alkaline solution and the alkali-activated compounds are precipitated. An empirical formula for these mineral polymers was formulated as $M_n[-(SiO_2)_z\text{-}AlO_2]_n \cdot wH_2O$, where z is 1, 2, or 3; M is an alkali cation as sodium or potassium, and n is the degree of polymerization. Three polymeric structures could be recognized from the resultant type of chemical bonding: poly(sialate) (–Si–O–Al–O), poly(sialate-siloxo) (Si–O–Al–O–Si–O), and poly(sialate-disiloxo) (Si–O–Al–O–Si–O–Si–O–) [1]–[4].

A wide range of solid materials can be applied as precursor materials in alkali-activated production, for example, the bottom ash, rice husk, palm oil fuel ash, ground granulated blast furnace, metakaolin, fly ash, among others [5]–[8]. However, several studies have focused on reactive fly-ashes and metakaolin – well-established precursors [9]–[11]. The metakaolin-based alkali-activated have the disadvantage of extensive shrinkage and cracking, while some kinds of fly ash require heat treatment to achieve high early strength and faster setting time of the resultant alkali-activated pastes, as well as the dark appearance of pulverized fly ash can be an issue when used for building restoration [12], [13]. Furthermore, due to their limited availability, researchers have started to study the application of other residues such as mine tailings [14], [15].

The alkali activation of mine tailings is considered a feasible and alternative method for sustainable management and an interesting alternative to the well-established precursors. The recycling and valorization of mine tailings have been pointed out as one of the most effective strategies to minimize their tremendous volume and negative environmental impacts. Indeed, the alkali activation technology – among the recent sustainable management strategies – offers many advantages, such as (i) valorization of the volume of tailings in the construction industry, (ii) stabilization of polluted/inert mine tailings in the alkali-activated matrix, and (iii) reduction of greenhouse gas emissions generated using ordinary Portland cement (OPC) [16], [17].

In this context, there is a scarce number of studies using iron ore tailings (IOT) in the alkali-activated technology; and further, these tailings are generally applied as a blend or even as fine aggregate replacement in alkali-activated cement synthesized using the well-established precursors [18], [19]. On the other hand, using IOT in the construction industry is one way to produce green and sustainable products, as well as save landfill space and minimize the extraction of non-renewable materials [20]. Moreover, recent studies have shown that the IOT has interesting potential to produce several types of construction and building materials based on OPC – from sustainable paint to raw material to clinkerization [21]–[24].

The present paper focuses on the IOT use as a precursor material in formulating an alkali-activated based composite. Therefore, this paper aims to study the potential of IOT as a precursor material as well as the impact of a dispersed phase (fine aggregate). The first phase of the study focused on specifying the set of parameters for alkali activation, such as grinding time, concentration of the alkaline solution, and temperature of curing. In the second phase, the obtained parameters were used to produce paste and mortars specimens, and the resulting composites were submitted to physical and mechanical strength tests.

3 MATERIALS AND EXPERIMENTAL PROGRAM

3.1 Materials

The IOT used in this paper was collected from a tailings dam located in Minas Gerais State, Brazil. The quartz sand was used as fine aggregate for mortars production, and NaOH pellets with purity >98% were used for the alkaline activator production.

The chemical composition of the IOT and quartz sand, obtained by X-ray fluorescence (XRF), on a Panalytical Epson^{3x} X-ray spectrometer, is shown in Table 1. The main elements of the IOT are iron oxide (48%), silica (40%), and alumina (8%). The quartz sand presented mostly silica (78%), alumina (10%), and iron oxide (6%). A long setting time is expected based on IOT's chemical composition and criteria of SiO_2/Al_2O_3 ratio [25]. It should be noted that IOT has a considerable amount of iron oxide, which could act in alkali-activated structure – the similarity of Fe^{3+} with Al^{3+} explains why Fe^{3+} ions act as network former occupying the tetrahedral sites [26]–[28].

Regarding the mineralogical compositions, the X-ray diffraction (XRD) of the IOT detected the presence of chamosite, chantalite, quartz, goethite, and hematite, while the quartz sand presented quartz, microcline, periclase, and biotite. The diffractogram of IOT and quartz sand showed no presence of a characteristic halo related to the amorphous phases, indicating a high crystallinity of these materials (Figure 1). The mineralogy of IOT is like those reported in the literature [29], [30] and its well-crystalline mineralogy could be associated with a non-reactivity or a low degree of reactivity [17].

Table 1. Chemical composition of iron ore tailings and quartz sand.

Major elements as oxide	Raw materials	
	IOT (wt%)	Quartz sand (wt%)
MgO	0.17	-
Al_2O_3	8.78	10.80
SiO_2	40.09	78.50
P_2O_5	0.55	-
K_2O	0.29	1.70
CaO	0.14	0.70
TiO_2	0.13	1.00
Fe_2O_3	48.97	6.00
MnO	0.42	0.10
Al_2O_3/SiO_2 (wt%/wt%)	0.21	-
Si/Al (atomic ratio)	4.03	-

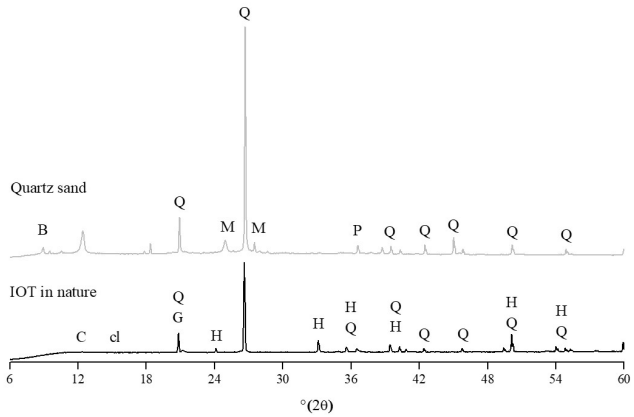

Figure 1. XRD pattern of the iron ore tailing in nature and quartz sand (B-biotite; C-chamosite; cl-chantalite; Q-quartz; G-goethite; H-hematite; M-microcline; P-periclase).

A sodium hydroxide solution was used as the alkaline activator and prepared in five molar concentrations: 6, 8, 10, 12, and 15 M (mol/L). It was prepared by dissolving NaOH pellets in deionized water.

Mortar composites were produced using the IOT and quartz sand as fine aggregate. The fine aggregate was particle separated by sieving in four equal fractions (2.4 – 1.2 mm; 1.2 – 0.6 mm; 0.6 – 0.3 mm; 0.3 – 0.15 mm) in accordance with ABNT NBR 7214 [31]. The fine aggregate was oven-dried at 105°C for 24 h to ensure a saturated surface dry (SSD) condition.

3.2. Experimental Program

As the IOT is not a common precursor or blend material to alkali-activated production, the experimental program was conducted in two phases – to understand the effects of IOT activation and to set the base parameters for the alkali-activated production. The experimental program and the tested parameters are schematized in Figure 2 and were based on the previous investigations [15], [32], [33].

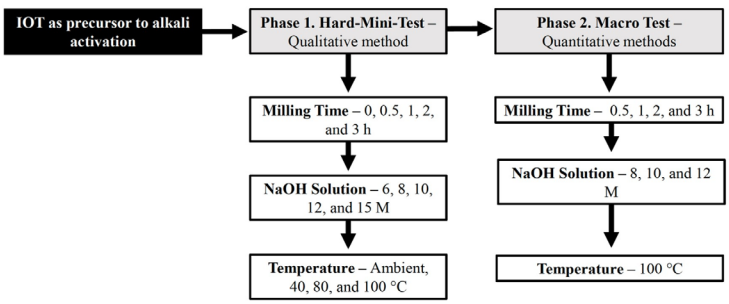

Figure 2. Schematic of the experimental program.

Two different types of mixture were tested: paste and mortar (see Table 2). The study of the pastes allowed the qualitative observation of reactivity and hardening properties of the IOT as a precursor material (Subtopic 3.2.1) and allowed to set base parameters. On the other hand, the study of the mortars allowed the quantitative experiment of the mechanical and microstructural properties of the composites produced using the IOT as the precursor material, as well as the effects of fine aggregate (Subtopic 3.2.2). An activator/precursor (A/P) ratio of 0.27 in mass was used for pastes and mortars to maintain suitable workability for all the investigated mixtures. A precursor/aggregate (P/Agg) ratio of 1:3, 1:2, and 1:0.5 was tested and, since the proportions of 1:3 and 1:2 did not show any cohesion in the flow table, was adopted the mix proportion of 1:0.5 was adopted for mortar specimens. Note that a paste with equal parameters (control) was prepared using only IOT and the alkaline activator to understand the role of fine aggregate on the composite properties.

Table 2. Mixture design of alkali-activated composites.

Phase	Type	Mixture ID	Material		A/P[c] (-)	P/Agg[d] (-)
			IOT (g)	Quartz sand (g)		
1	Paste	P-6-0 to P-15-3[a,b]	20.00	-	0.27	-
2	Paste	P-8-1 to P-12-3[a,b]	1500.00	-	0.27	-
	Mortar	M-8-1 to M-12-3[a,b]	1100.00	550.00		1:0.5

[a] X-Y-W, where X denotes the type, Y denotes the concentration of the alkaline activator, and W denotes grinding time. [b] Including all specimens inside this range. [c] Activator/precursor. [d] Precursor/aggregate ratio.

3.2.1 Hard-Mini-Test (HMT)

In Phase 1, the hardening aspect of the IOT-based alkali-activated was qualitatively observed using a combination of three parameters: i) temperature of curing, ii) grinding time, and iii) concentration of alkaline activator. The thermal curing conditions were ambient temperature (23 ± 2°C), 40, 80, and 100 °C. The IOT was ground in a horizontal ball mill (MARCONI instrument) for 30 min, 1, 2, and 3 h, and the particle size distribution of the milled IOT was determined using a laser diffraction analyzer (BETTERSIZE 2000 instrument). The effect of the concentration of the alkaline activator was observed using concentrations of 6, 8, 10, 12, and 15 M (mol/L). The combination of these three parameters produced 100 miniature specimens, which were used to evaluate the hardening properties of the IOT applying the alkaline activation method.

The preparation of the pastes began with the manually mixing of the IOT and alkaline activator for 5 min until complete homogenization. The resulting paste was then placed in a cylindrical polyvinyl chloride mold of diameter 20 mm and height 40 mm. Then the specimens were covered with plastic film to prevent evaporation during the curing process.

3.2.2 Macro test

In Phase 2, specific parameters were selected and used for quantitative tests in regular sizes (i.e., regular sizes according to specific standards). Based on the qualitative results observed in Phase 1 were chosen the set range of parameters: i) thermal curing of 100°C, ii) 1, 2, and 3 h of grinding, and iii) solution concentration of 8, 10, and 12 M. The applied criterion to choose the set of parameters will be discussed in detail in the following Subtopic 4.1.

In Phase 2, paste and mortar specimens were used. The preparation of these specimens was carried out in a laboratory mixer (JJ-5 Type), where first was homogenized the IOT and fine aggregate in a plastic container for 5 min. Then added the alkaline activator to the mixer bowl and solid materials (IOT and fine aggregate). Then, they were mixed for 3 min at low speed, paused for 30 s to scrap the mixer shovel, and mixed for 3 min at high speed. The fresh mortars were placed in stainless prismatic molds, with dimensions 40 × 40 × 160 mm and covered with a glass plate to prevent evaporation during the curing process. The same preparation process was applied to the paste specimens, except homogenization of IOT and fine aggregate. Thermal curing was carried out in a laboratory oven, and the temperature of the alkaline activator at the mixing time was 23±2 °C.

Both pastes and mortars were cured for 7 days inside the molds at 100°C. After curing, their properties were determined, and each specimen was weighed and measured shortly before being tested. Results showed in this study represent the average of a specific number of tested specimens as better described hereafter. The physical and mechanical properties of the alkali-activated composites were obtained using the following methods:

i. The dimensional stability was determined by measuring the length of each specimen. The final dimensions of the specimens were measured using a caliper after the curing period. The average of the results of three specimens was taken for each mixture. The length change percentage was calculated using Equation 1.

$$Length\ Change\ (\%) = \left[\frac{(L1-L2)}{L1}\right].100 \quad (1)$$

where L1 is the reference length of the prismatic mold, and L2 is the length of the specimen, measured after the curing period.

ii. The nominal sample density was measured prior to the flexural strength test. The average value was calculated from three samples. The calculations were performed according to Equation 2.

$$Nominal\ sample\ density\ (g \cdot cm^{-3}) = \frac{W}{V} \quad (2)$$

where W and V are the weight and volume of the sample after the curing period, respectively.

iii. The 7-days flexural and compressive strength tests were performed in accordance with NBR 13279 [34]. Three specimens of each mixture were used for the flexural strength test and six specimens of each mixture were used for the compressive strength test. The tests were carried out using a hydraulic press (EMIC DL 2000 instrument) with a load cell of 200 kN and a load increment of 0.25 MPa·s^{-1}.

iv. The water absorption tests were carried out in fragments collected from the specimens used in the mechanical tests and based on ASTM C67-07 [35]. The water absorption percentages were calculated using Equation 3.

$$Water\ absorption\ (\%) = \left[\frac{(W_{SSD}-W_d)}{W_d}\right].100 \quad (3)$$

where W_d is the dry weight of the sample and W_{SSD} is the weight of the sample after 48 h soaking in water (SSD condition).

4 RESULTS AND DISCUSSIONS

4.1 HMT characterization

The effect of grinding time on IOT particle fineness is shown in Figure 3. The grinding process yields a 56% reduction from 229.8 to 101.0 mm, considering the maximum size of the IOT. It can be observed that the IOT in nature shows a D90 of 172.9 mm, while the IOT ground for 30 min, 1, 2, and 3 h shows a D90 of 96.3, 76.6, 71.1, and 51.0 mm, respectively. As reported before, the mechanical properties of rice husk ash-based alkali activated depend on an array of factors, such as the particle size distribution of the precursor material. Moreover, the effect of particle size observed in fly ash-based alkali-activated is more pronounced at low temperatures and the reaction mechanism of early activation (i.e., nucleation and growth) does not alter with the change of particle fineness [36]. However, it is well stated that the fineness of the precursor materials leads to compact microstructure development and improved properties [37]–[39], which is confirmed in Subtopic 4.2 when analyzing the mechanical strength results.

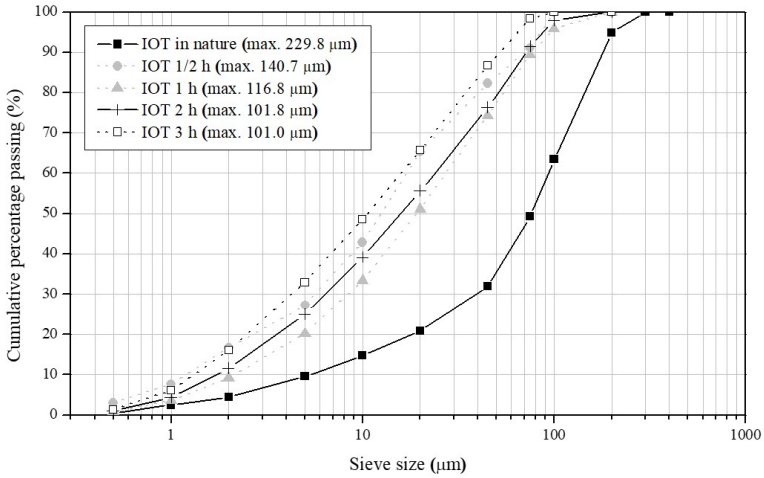

Figure 3. Grading of iron ore tailings.

The qualitative results of the HMT tests are summarized in Table 3. It can be observed that the ambient temperature and temperature of 40 and 80°C were not sufficient for the alkaline activation of IOT – as the specimens not hardened at 7 days of curing. The concentration of alkaline activator of 6M was the unique parameter that showed at least one specimen that did not harden at 7 days at 100°C of thermal curing. These not-hardened specimens showed plastic deformation to the finger touch. Furthermore, it should be noted that the temperature degree was more effective than grinding time on the IOT reactivity and hardening property. It is notorious the effect of the thermal curing parameter, as previously observed by Ahmari and Zhang [15], Somna et al. [40] and Mehta and Siddique [41], since at high temperatures, there is an increase in dissolution of Si and Al oxides from the precursor material.

The alkaline activator concentration also had an interesting effect on the hardening properties. It was observed that the lowest alkaline concentration (i.e., 6 M) was not enough to harden, while a hardening effect was observed at all other alkaline concentrations – even at a lower temperature such as 80°C. It was found that the setting time increases as the alkaline concentration increases until an optimum limit, which could be related to the observed results [42], [43].

Based on these results, the temperature parameter of 100°C was chosen since all the specimens hardened for this condition. The molar concentration of 6M was excluded since some specimens did not harden. The concentration of 15M was also excluded since the results did not justify the high consumption. Furthermore, since not all specimens ground for 0 and 30 min have hardened, they were also excluded from Phase 2, thus resulting in the set of parameters presented in Subtopic 3.2.2.

Table 3. Hard-mini-test (HMT) results at 7 days of curing.

Mixture ID[a]	Temperature °C				Mixture ID	Temperature °C				Mixture ID	Temperature °C			
	22	40	80	100		22	40	80	100		22	40	80	100
P-6-0	*X*	*X*	*X*	*X*	P-10-0	*X*	*X*	*X*	✓	P-15-0	*X*	*X*	*X*	✓
P-6-1/2	*X*	*X*	*X*	*X*	P-10-1/2	*X*	*X*	*X*	✓	P-15-1/2	*X*	*X*	*X*	✓
P-6-1	*X*	*X*	*X*	✓	P-10-1	*X*	*X*	*X*	✓	P-15-1	*X*	*X*	*X*	✓
P-6-2	*X*	*X*	*X*	✓	P-10-2	*X*	*X*	*X*	✓	P-15-2	*X*	*X*	*X*	✓
P-6-3	*X*	*X*	*X*	✓	P-10-3	*X*	*X*	✓	✓	P-15-3	*X*	*X*	✓	✓
P-8-0	*X*	*X*	*X*	✓	P-12-0	*X*	*X*	*X*	✓					
P-8-1/2	*X*	*X*	*X*	✓	P-12-1/2	*X*	*X*	*X*	✓					
P-8-1	*X*	*X*	*X*	✓	P-12-1	*X*	*X*	*X*	✓					
P-8-2	*X*	*X*	✓	✓	P-12-2	*X*	*X*	*X*	✓					
P-8-3	*X*	*X*	✓	✓	P-12-3	*X*	*X*	✓	✓					

The abbreviation *X* means specimens that have not hardened. The abbreviation ✓means specimens that have hardened. [a] P-Y-W, where P denotes paste, Y denotes the concentration of the alkaline activator, and W denotes grinding time

4.2. Macro Properties

4.2.1 Physical properties

Dimensional stability is usually considered a significant durability parameter for construction and building materials as it suggests the potential for cracking in the hardened state. The dimensional stability of the alkali-activated specimens, reported in terms of length change, is shown in Figure 4. It was observed that the paste specimens showed length change values between 3.1 and 7.2%, while the mortar specimens showed values between 1.0 and 2.7%. The addition of fine aggregate reduced the length change by over 35% when compared against the paste specimens. This reduction could be due to the fine aggregate particles that limit shrinkage by forming a supportive network with a fixed void volume. Overall, the results are significantly higher than those observed from alkali-activated materials derived from industrial wastes and metakaolin [40], [41].

The results also reveal that the grinding time is a key parameter in length change behavior. It should be noted that the length change is directly proportional to the grinding time in paste specimens. For example, it was noted that from 1 to 3h of grinding, the specimens showed an increase of 71% from 3.5 to 6.0%. On the other hand, for the mortar specimens, the increase in grinding time did not significantly alter the length change, suggesting that, in this case, the dimensional stability is governed by the fine aggregate supportive network.

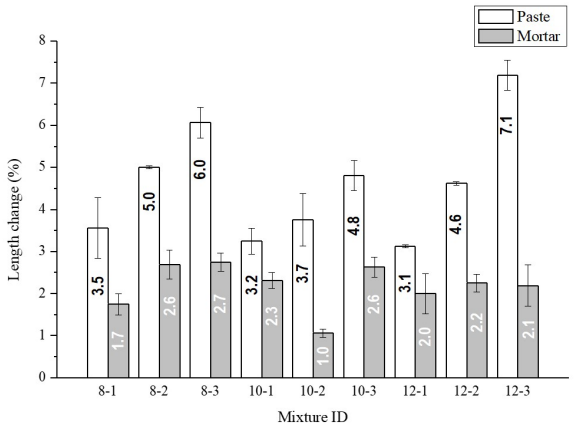

Figure 4. Length change of alkali-activated specimens.

Results of nominal sample density are shown in Figure 5. The paste specimens showed density values between 1.9 and 2.4 g·cm^{-3}, while the mortar specimen values were between 2.1 and 2.2 g·cm^{-3}. That is a non-surprising behavior given the shrinkage effect and the obtained values are in good agreement with values of clay bricks (between 1.8 to 2.0 g·cm^{-3}) [44] and strain hardening geopolymer composite (between 1.8 to 1.9 g·cm^{-3}) [45]. Meanwhile, paste and mortars density values were higher than fly ash-based alkali-activated, whose range was between 1.5 and 1.6 g·cm^{-3} [46].

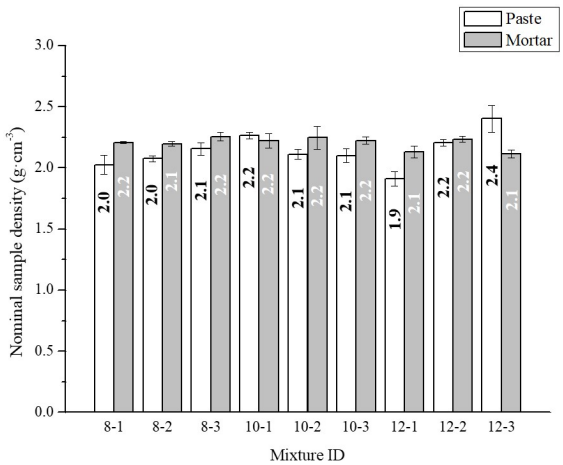

Figure 5. Nominal sample density of alkali-activated specimens.

4.2.2 Mechanical properties

The average 7-days flexural and compressive strengths for each mix are shown in Figure 6. The results showed that 7-days flexural strength for the paste specimens varied between 2.4 and 25.1 MPa, while mortars varied between 4.0 and 11.1 MPa. The addition of fine aggregate decreased the flexural strength, except for the specimens 12-1, 12-2, and 12-3 (12 M and 1, 2, and 3 h of grinding time, respectively). This result could be related to the increase in volume and porosity, as expected in composites with binder and dispersed phase (mortars), which are more sensitive to tensile stress. Moreover, the obtained results were slightly higher when compared to a few alkali-activated mortars based on metakaolin and fly-ash [47], [48].

Compressive strength is a key feature for construction and building materials and an interesting parameter to associate with alkaline activation – quality and amount of alkali-activated products. The 7-days compressive strength of the paste specimen values was between 19.0 and 110.0 MPa, while the mortars were between 26.0 and 67.0 MPa. In general, adding fine aggregates reduced the compressive strength by over 15%, except for the 75% increase observed in specimens 8-1. These results are like those reported by Tchakouté and Rüscher [49] and Hu et al. [50] for metakaolin- and fly ash-based alkali-activated, demonstrating the potential of IOT as a promising precursor material. Moreover, the higher mechanical performance of paste than mortars was also observed by Cristelo et al. [51], which probably was associated with differences in porosity and compaction.

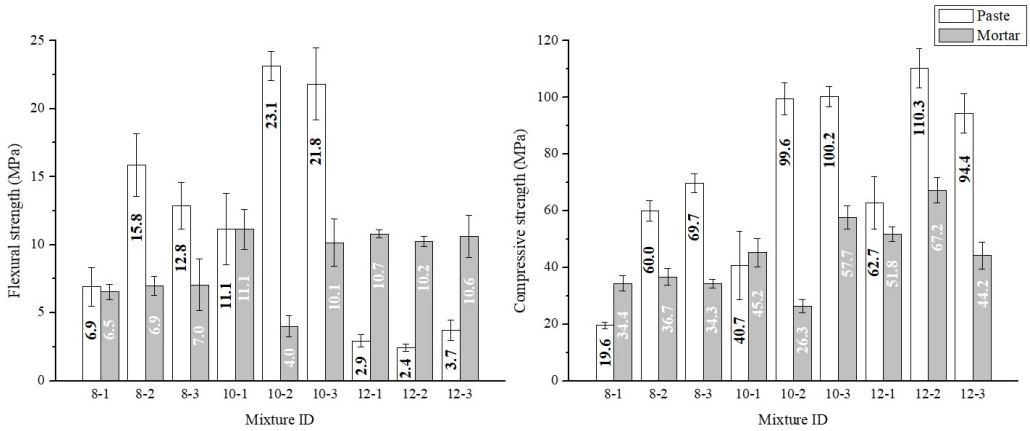

Figure 6. Mechanical properties of alkali-activated specimens at 7 days of curing.

The effect of the concentration of the alkaline activator on the compressive strength was important for paste and mortar specimens. Hence, as the molar concentration increased to the optimal content, the compressive strength of specimens also increased, reaching a maximum value. This effect may be related to the rate and degree of alkaline activation, which is facilitated by an increase in the alkaline activator concentration. It also can be observed for both alkali-activated type specimens that the optimal concentration was 12 M.

The increase in compressive strength was noteworthily influenced by the particle size distribution of the IOT, as evidenced by the results of the laser particle analyzer. The compressive strength increased by over 90% from 1 to 2 h of grinding time for paste specimens. However, the grinding time appears to be more effective in low concentration of alkaline activator (8M), suggesting that the high alkalinity overpass the effect of the IOT's particle fineness in the alkali-activated reaction. For example, the increase from 2 to 3 h of grinding time yield a 16% increase (from 60.0 to 69.7 MPa) in specimens activated with the 8M solution, while for specimens activated with the 12M solution, the same increase led to a 14% reduction. These results showed that the grinding method probably leads to finer and more homogeneous particles causing faster dissolution of reactive Si and Al pieces [17], [52].

It should be noted that the mortar specimen showed compressive strength slightly influenced by the IOT particle size distribution and was ruled by the pack arrangement due to the particle size distribution of the fine aggregate. These results agree with the effect of particle size distribution on mechanical behavior and specimen density.

After the compressive strength test, the specimens were collected for the water absorption test (Figure 7). The paste specimens showed a water absorption between 3.1 and 13.5%, while mortar specimens showed values between 2.3 and 10.6%. In general, the use of fine aggregate decreased water absorption values compared to the paste specimens. This decrease in water absorption could be the first sign that the use of fine aggregate did not generate greater porosity in

the mortar specimens or, even if it did, the interconnectivity of the pores was low. The results of water absorption are consistent with previous research [53].

The water absorption of an alkali-activated composite depends on its chemical nature, structural morphology, and volume of pores. A higher degree of alkaline activation can lead to a denser and less permeable composite. It could be observed that the mortar specimens 8-1, 10-1, and 12-1 disintegrated after soaking in water. This fact might indicate that the specimens were in the lag phase (induction period) and showed a lack of sufficient structural integrity [54]. On the other hand, since this fact undergoes only in mortar specimens, this also might be related to differences in the alkali-activated reaction due to the presence of a dispersed phase in the composite.

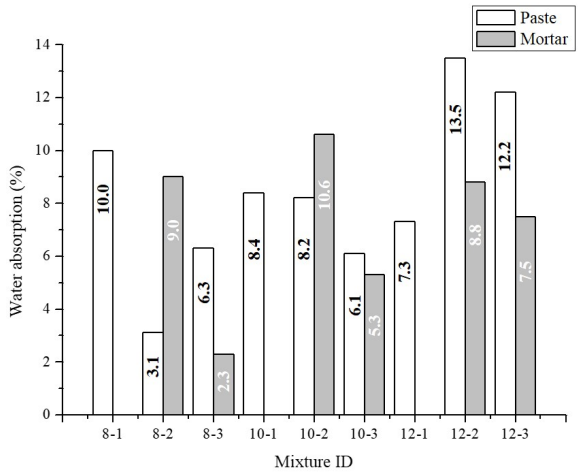

Figure 7. Water absorption of alkali-activated specimens.

4.2.3 Alkali-activated technology applied in iron ore tailings

The results obtained in both pastes and mortars show that IOT can be an interesting precursor to the manufacture of alkali-activated materials, resulting in the development of composites with high mechanical performance. The results show promising opportunities for IOT as the main precursor in alkali-activated technology.

There is a wide range of opportunities regarding using these composites as a construction and building material. According to the American Standards (ASTM), the composite based on IOT easily achieves the minimum strength of building bricks (20.7 MPa) [55], pedestrian and light traffic (55.2 MPa) [56], and the maximum water absorption (17% and 8%, respectively). Furthermore, the mechanical properties of pastes and mortars were superior to the Portland cement high-performance concrete (55.0 MPa), consuming a hard-to-manage tailing and yielding an eco-friendly composite.

5 CONCLUSIONS

The study investigated the effect of four major factors on the physical and mechanical properties of the IOT-based composites: i. the concentration of alkaline activator, ii. the particle size distribution of precursor material, iii. the temperature of curing, and iv. the use of fine aggregate. Through the experimental results, the main conclusions obtained in this paper are:

I. Using IOT as the precursor material to the alkali-activated process yielded composites with 7-days compressive and flexural strengths of 110.0 and 25.0 MPa, respectively. These results were greatly influenced by the concentration of the alkaline activator and the grinding time.

II. The temperature and alkaline concentration were controlling factors in the alkaline activation of IOT. The alkaline solution of 6 M was not sufficient to harden even at 100°C, while the temperature time played a key role in the alkaline activation. Furthermore, the grinding procedure seems to be an interesting alternative route rather than high molarity solutions.

III. Alkali-activated mortars also showed high strength values – 7-days compressive and flexural strength values reached 67.0 and 11.0 MPa, respectively. In general, the mortars showed strength reductions ranging from 15 to 40% compared to the corresponding alkali-activated pastes.

IV. The alkali-activated pastes showed high length change, while the fine aggregate in the mortar specimens significantly reduced this effect. In general, the mortars also showed a decrease in water absorption when compared to the paste specimens. Both IOT paste and mortar specimens met the ASTM requirements for diverse construction and building materials.

V. The results showed promising applications of IOT as a construction and building material with appropriate mix proportions and activation process. The availability available and safety concerns related to the storage of IOT encourage its application as the precursor or even as a blend material to alkali-activated composites.

Few barriers such as water resistance, variability in composition, application of alkaline solutions, uncertainty in the exact degree of alkaline activation, and thermal curing may cause difficulties in widespread practical applications of this alkali-activated type. In this sense, the present work contributes to a more in-depth discussion and understanding of IOT reactivity, as well as the properties of IOT-based composites. However, additional research is needed for a more in-depth investigation of the effect of compaction, alkaline activation degree, and durability.

ACKNOWLEDGEMENTS

We gratefully acknowledge the agencies CAPES, FAPEMIG, and CNPq for providing financial support. We are also grateful for the infrastructure and collaboration of the research groups RECICLOS-CNPq, ATIVE-CNPq, and SICon-CNPq.

The authors also would like to acknowledge the Nanolab Laboratory at the REDEMAT - UFOP, for providing the equipment and technical support for XRD experiments, Civil Materials Construction Laboratory at the Department of Civil Engineering, Federal University of Ouro Preto, for the infrastructure and equipment.

REFERENCES

[1] J. Davidovits, "Geopolymers: inorganic polymeric new materials," *J. Therm. Anal.*, vol. 37, no. 8, pp. 1633–1656, 1991.

[2] B. Majidi, "Geopolymer technology, from fundamentals to advanced applications: a review," *Mater. Technol.*, vol. 24, no. 2, pp. 79–87, 2009.

[3] N. Elmesalami, and K. Celik, "A critical review of engineered geopolymer composite: a low-carbon ultra-high-performance concrete," *Constr. Build. Mater*., vol. 346, pp. 128491, 2022.

[4] O. Wan-En et al., "Towards greener one-part geopolymers through solid sodium activators modification," *J. Clean. Prod.*, vol. 378, pp. 134370, 2022.

[5] F. Okoye, J. Durgaprasad, and N. Singh, "Mechanical properties of alkali activated fly ash/Kaolin based geopolymer concrete," *Constr. Build. Mater.*, vol. 98, no. 15, pp. 685–691, 2015.

[6] P. Choeycharoen, W. Sornlar, and A. Wannagon, "A sustainable bottom ash-based alkali-activated materials and geopolymers synthesized by using activator solutions from industrial wastes," *J. Build. Eng.*, vol. 54, pp. 104659, 2022.

[7] Sk. Hossain, P. Roy, and C. Bae, "Utilization of waste rice husk ash for sustainable geopolymer: a review," *Constr. Build. Mater.*, vol. 310, pp. 125218, 2021.

[8] S. Kabir, U. J. Alengaram, M. Z. Jumaat, S. Yusoff, A. Sharmin, and I. I. Bashar, "Performance evaluation and some durability characteristics of environmentally friendly palm oil clinker based geopolymer concrete," *J. Clean. Prod.*, vol. 161, no. 10, pp. 477–492, 2017.

[9] V. Trincal et al., "Shrinkage mitigation of metakaolin-based geopolymer activated by sodium silicate solution," *Cement Concr. Res.*, vol. 162, pp. 106993, 2022.

[10] J. van Jaarsveld, J. van Deventer, and G. Lukey, "The effect of composition and temperature on the properties of fly ash- and kaolinite-based geopolymers," *Chem. Eng. J.*, vol. 28, no. 1-3, pp. 63–73, 2002.

[11] J. Cai, X. Li, J. Tan, and B. Vandevyvere, "Thermal and compressive behaviors of fly ash and metakaolin-based geopolymer," *J. Build. Eng.*, vol. 30, pp. 101307, 2020.

[12] P. Chindaprasirt, C. Jaturapitakkul, W. Chalee, and U. Rattanasak, "Comparative study on the characteristics of fly ash and bottom ash geopoylmers," *Waste Manag.*, vol. 2, no. x, pp. 539–543, 2009.

[13] C. Künzel, C. Cheeseman, L. Vandeperre, and A. Boccaccini, "An assessment of drying shrinkage in metakaolin-based geopolymer," *J. Am. Ceram. Soc.*, vol. 95, pp. 3270–3277, 2012.

[14] P. Ken, M. Ramli M and C. Ban, "An overview on the influence of various factors on the properties of geopolymer concrete derived from industrial by-products," *Constr. Build. Mater.*, vol. 77, pp. 370–395, 2015.

[15] S. Ahmari and L. Zhang, "Production of eco-friendly bricks from copper mine tailings through geopolymerization," *Constr. Build. Mater.*, vol. 29, pp. 323–331, 2012.

[16] X. He, Z. Yuhua, S. Qaidi, H. F. Isleem, O. Zaid, F. Althoey, and J. Ahmad, "Mine tailings-based geopolymers: a comprehensive review," *Ceram. Int.*, vol. 48, no. 17, pp. 24192–24212, 2022.

[17] S. Mabroum, S. Moukannaa, A. El Machi, Y. Taha, M. Benzaazoua, and R. Hakkou, "Mine wastes based geopolymers: a critical review," *Clean Eng Tech.*, vol. 1, pp. 100014, 2020.

[18] Z. Lu and M. Cai, "Disposal methods on solid wastes from mines in transition from open-pit to underground mining," *Procedia Environ. Sci.*, vol. 16, pp. 715–721, 2012.

[19] P. Duan, C. Yan, W. Zhou and D. Ren, "Development of fly ash and iron ore tailings based porous geopolymer for removal of Cu(II) from wastewater," *Ceram. Int.*, vol. 42, no. 12, pp. 13507–13518, 2016.

[20] P. Duan, C. Yan, W. Zhou and D. Ren, "Fresh properties, compressive strength and microstructure of fly ash geopolymer paste blended with iron ore tailing under thermal cycle," *Constr. Build. Mater.*, vol. 118, pp. 76–88, 2016.

[21] Z. Ismail and E. Al-Hashimi, "Reuse of waste iron as a partial replacement of sand in concrete," *Waste Manag.*, vol. 28, no. 11, pp. 2048–2053, 2008.

[22] S. Zhao, J. Fan, and W. Sun, "Utilization of iron ore tailings as fine aggregate in ultra-high performance concrete," *Constr. Build. Mater.*, vol. 32, pp. 540–548, 2013.

[23] J. Franco de Carvalho, P. A. M. Campos, K. Deváveri, G. J. Brigolini, L. G. Pedroti, and R. A. F. Peixoto, "Low environmental impact cement produced entirely from industrial and mining waste," *J. Mater. Civ. Eng.*, vol. 31, no. 2, pp. 040018391, 2019.

[24] J. Galvao, H. D. Andrade, G. J. Brigolini, R. A. F. Peixoto, and J. C. Mendes, "Reuse of iron ore tailings from tailings dams as pigment for sustainable paints," *J. Clean. Prod.*, vol. 200, pp. 412–422, 2018.

[25] P. De Silva, K. Sagoe-Crenstil, and V. Sirivivatnanon, "Kinetics of geopolymerzation: role of Al2O3 and SiO2," *Cement Concr. Res.*, vol. 37, no. 4, pp. 512–518, 2007.

[26] Y. Hu et al., "Role of Fe species in geopolymer synthesized from alkali-thermal pretreated Fe-rich Bayer red mud," *Constr. Build. Mater.*, vol. 200, pp. 398–407, 2019.

[27] N. Ye et al., "Transformations of Na, Al, Si and Fe species in red mud during synthesis of one-part geopolymers," *Cement Concr. Res.*, vol. 101, pp. 123–130, 2017.

[28] P. Lemougna, K. J. D. MacKenzie, G. N. L. Jameson, H. Rahier & U. F. Chinje Melo, "The role of iron in the formation of inorganic polymers (geopolymers) from volcanic ash: a 57Fe Mössbauer spectroscopy study," *J. Mater. Sci.*, vol. 48, no. 15, pp. 5280–5286, 2013.

[29] V. Piffer, K. Soares, and A. Galdino, "Evaluation of mechanical and thermal properties of PP/iron ore tailing composites," *Compos. Part B*, vol. 221, pp. 109001, 2021.

[30] P. Dauce, G. B., Castro, M. M. F. Lima, and R. M. F. Lima, "Characterisation and magnetic concentration of an iron ore tailings," *J. Mater. Res. Technol.*, vol. 8, no. 1, pp. 1052–1059, 2019.

[31] Associação Brasileira de Normas Técnicas, *Standard Sand for Cement Tests – Specification*, ABNT NBR 7214, 2015.

[32] F. Pacheco-Torgal, D. Moura, Y. Ding, & S. Jalali, "Composition, strength and workability of alkali-activated metakaolin based mortars," *Constr. Build. Mater.*, vol. 25, no. 9, pp. 3732–3745, 2011.

[33] S. Jeeva Chithambaram, S. Kumar, and M. Prasad, "Thermo-mechanical characteristics of geopolymer mortar," *Constr. Build. Mater.*, vol. 213, pp. 100–108, 2019.

[34] Associação Brasileira de Normas Técnicas, *Mortars applied on wall and ceilings – Determination of the flexural and the compressive strength in the hardened stage*, ABNT NBR 13279, 2015.

[35] American Society for Testing and Materials, *Standard Test Methods for Sampling and Testing Brick and Structural Clay Tile*, ASTM C67-07, 2007.

[36] S. Nath and S. Kumar, "Reactions kinetics of fly ash geopolymerization: Role of particle size controlled by using ball mill," *Adv. Powder Technol.*, vol. 30, no. 5, pp. 1079–1088, 2019.

[37] S. Kumar, F. Kristály, and G. Mucsi, "Geopolymerisation behaviour of size fractioned fly ash," *Adv. Powder Technol.*, vol. 26, no. 1, pp. 24–30, 2015.

[38] L. Assi, E. Deaver, and P. Ziehl, "Effect of source and particle size distribution on the mechanical and microstructural properties of fly Ash-Based geopolymer concrete," *Constr. Build. Mater.*, vol. 167, pp. 372–380, 2018.

[39] Z. Li, Y. Gao, J. Zhang, C. Zhang, J. Chen, and C. Liu, "Effect of particle size and thermal activation on the coal gangue based geopolymer," *Mater. Chem. Phys.*, vol. 267, pp. 124657, 2021.

[40] K. Somna, C. Jaturapitakkul, P. Kajitvichyanukul, and P. Chindaprasirt, "NaOH-activated ground fly ash geopolymer cured at ambient temperature," *Fuel*, vol. 22, no. 6, pp. 2118–2124, 2011.

[41] A. Mehta and R. Siddique, "An overview of geopolymers derived from industrial by-products," *Constr. Build. Mater.*, vol. 127, pp. 183–198, 2016.

[42] J. Cai., J. Pan, J. Han, Y. Lin, and Z. Sheng, "Impact behaviours of engineered geopolymer composite exposed to elevated temperatures," *Constr. Build. Mater.*, vol. 312, pp. 125421, 2021.

[43] J. Cai, J. Pan, J. Han, Y. Lin, and Z. Sheng, "Low-energy impact behavior of ambient cured engineered geopolymer composites," *Ceram. Int.*, vol. 48, no. 7, pp. 9378–9389, 2022.

[44] K. Lin, "Feasibility study of using brick made from municipal solid waste incinerator fly ash slag," *J. Hazard. Mater.*, vol. 137, no. 3, pp. 1810–1816, 2006.

[45] B. Nematollahi, J. Sanjayan, J. Qiu, and E.-H. Yang, "Micromechanics-based investigation of a sustainable ambient temperature cured one-part strain hardening geopolymer composite," *Constr. Build. Mater.*, vol. 131, pp. 552–563, 2017.

[46] G. Gorhan and G. Kurklu, "The influence of the NaOH solution on the properties of the fly ash-based geopolymer mortar cured at different temperatures," *Compos. Part B.*, vol. 58, pp. 371–377, 2013.

[47] M. Al-Majidi, A. Lampropoulos, A. Cundy, and S. Meikle, "Development of geopolymer mortar under ambient temperature for in situ applications," *Constr. Build. Mater.*, vol. 120, pp. 192–211, 2016.

[48] K. Onoue, Y. Sagawa, D. Atarashi, and Y. Takayama, "Optimization of mix proportions and manufacturing conditions of fly-ash-based geopolymer mortar by parameters design with dynamic characteristics," *Cement Concr. Compos.*, vol. 133, pp. 104645, 2022.

[49] H. Tchakouté and C. Rüscher, "Mechanical and microstructural properties of metakaolin-based geopolymer cements from sodium waterglass and phosphoric acid solution as hardeners: a comparative study," *Appl. Clay Sci.*, vol. 149, pp. 81–87, 2017.

[50] W. Hu, Q. Nie, B. Huang, X. Shu, and Q. He, "Mechanical and microstructural characterization of geopolymers derived from red mud and fly ashes," *J. Clean. Prod.*, vol. 186, pp. 799–806, 2018.

[51] N. Cristelo, J. Coelho, T. Miranda, Á. Palomo, and A. Fernández-Jiménez, "Alkali activated composites – Na innovative concept using iron and steel slag as both precursor and aggregate," *Cement Concr. Compos.*, vol. 103, pp. 43–47, 2019.

[52] X. Jiao, Y. Zhang, and T. Chen, "Thermal stability of a silica-rich vanadium tailings based geopolymer," *Constr. Build. Mater.*, vol. 38, pp. 43–47, 2013.

[53] A. Wongsa, V. Sata, B. Nematollahi, J. Sanjayan, and P. Chindaprasirt, "Mechanical and thermal properties of lightweight geopolymer mortar incorporating crumb rubber," *J. Clean. Prod.*, vol. 195, pp. 1069–1080, 2018.

[54] J. Provis and J. van Deventer, *Geopolymers: Structure, Processing, Properties and Industrial Applications*, Boston, MA, USA: Woodhead Publishing Limited, 2009.

[55] American Society for Testing and Materials, *Standard Specification for Building Brick (Solid Masonry Units Made from Clay or Shale)*, ASTM C65-10, 2010.

[56] American Society for Testing and Materials, *Standard Specification for Pedestrian and Light Traffic Paving Brick*, ASTM C902-07, 2007.

Author contributions: KD: conceptualization, methodology, validation, formal analysis, investigation, data curation, writing, visualization; FE and JFC: validation, formal analysis, investigation, writing; RP and GS: conceptualization, visualization, funding acquisition, supervision, resources, project administration.

Editors: Fernando Pelisser, Guilherme Aris Parsekian.